The control of atmospheric pCO_2 by ocean ventilation change: The effect of the oceanic storage of biogenic carbon

Eun Young Kwon,[1] Jorge L. Sarmiento,[1] J. R. Toggweiler,[2] and Tim DeVries[3]

Received 16 February 2011; revised 5 May 2011; accepted 16 June 2011; published 29 September 2011.

[1] A simple analytical framework is developed relating the atmospheric partial pressure of CO_2 to the globally-averaged concentrations of respired carbon ($\overline{C_{soft}}$) and dissolved carbonate ($\overline{C_{carb}}$) in the ocean. Assuming that the inventory of carbon is conserved in the ocean-atmosphere system (i.e. no seawater-sediment interactions), the resulting formula of $\frac{\Delta pCO_2}{pCO_2} = -0.0053\Delta\ \overline{C_{soft}} + 0.0034\Delta\ \overline{C_{carb}}$ suggests that atmospheric pCO_2 would decrease by 5.3% and increase by 3.4% when $\overline{C_{soft}}$ and $\overline{C_{carb}}$ increase by 10 μmol kg^{-1}, respectively. Using this analytical framework along with a 3-D global ocean biogeochemistry model, we show that the response of atmospheric pCO_2 to changes in ocean circulation is rather modest because ~30% of the change in atmospheric pCO_2 caused by the accumulation of respired carbon is countered by a concomitant accumulation of dissolved carbonate in deep waters. Among the suite of circulation models examined here, the largest reduction in atmospheric pCO_2 of 44–88 ppm occurs in a model where reduced overturning rates of both southern and northern sourced deep waters result in a four-fold increase in the Southern Ocean deep water ventilation age. On the other hand, when the ventilation rate of the southern-sourced water decreases, but the overturning rate of North Atlantic Deep Water increases, the resulting decrease in atmospheric pCO_2 is only 14–34 ppm. The large uncertainty ranges in atmospheric pCO_2 arise from uncertainty in how surface productivity responds to circulation change. Although the uncertainty is large, this study suggests that a synchronously reduced rate for the deep water formation in both hemispheres could lead to the large glacial reduction in atmospheric pCO_2 of 80–100 ppm.

Citation: Kwon, E. Y., J. L. Sarmiento, J. R. Toggweiler, and T. DeVries (2011), The control of atmospheric pCO_2 by ocean ventilation change: The effect of the oceanic storage of biogenic carbon, *Global Biogeochem. Cycles*, *25*, GB3026, doi:10.1029/2011GB004059.

1. Introduction

[2] The world's deep waters accumulate and store carbon derived from the soft-tissue and carbonate pumps [*Volk and Hoffert*, 1985; *Anderson and Sarmiento*, 1994]. Figure 1 presents the distributions of respired carbon (C_{soft}) and dissolved carbonate (C_{carb}) in the ocean's interior, as estimated from the climatological data of nutrients, alkalinity and oxygen (see Appendix A and *Gruber and Sarmiento* [2002]). The ratio of C_{carb} to C_{soft} increases with increasing depth, ranging from ~0.2 in intermediate waters to ~0.5 in bottom waters. This is because while most sinking organic particles remineralize within the top 1000 m through heterotrophic respiration, the majority of biogenic $CaCO_3$ dissolves in deep waters below the saturation horizon [*Broecker and Peng*, 1987]. The preferential storage of dissolved carbonate in bottom waters results in a longer mean residence time of dissolved carbonate than respired carbon in the ocean's interior. As a result, the globally-averaged concentration of dissolved carbonate $\overline{C_{carb}} = 29 \pm 12$ μmol kg^{-1} is about one-third of the globally-averaged concentration of respired carbon $\overline{C_{soft}} = 103 \pm 20$ μmol kg^{-1} (see Appendix A), despite the fact that the global export of $CaCO_3$ is less than 10% of the export of organic carbon at the base of the euphotic zone [*Yamanaka and Tajika*, 1996; *Sarmiento et al.*, 2002; *Dunne et al.*, 2007; *Kwon and Primeau*, 2008].

[3] Most of the deep water enriched in biogenic carbon makes its first contact with the atmosphere in the Southern Ocean [*Toggweiler and Samuels*, 1995; *Gnanadesikan*, 1999; *Primeau*, 2005]. The biogenic carbon that upwells along with circumpolar deep water encounters two distinct fates depending on its return pathway to the deep water formation regions [*Toggweiler et al.*, 2006]. One pathway can be characterized as a circuit involving the northward flow of Subantarctic Mode Water and Antarctic Intermediate Water that feed into the North Atlantic Deep Water (NADW)

[1]Atmospheric and Oceanic Sciences Program, Princeton University, Princeton, New Jersey, USA.
[2]Geophysical Fluid Dynamics Laboratory, National Oceanic and Atmospheric Administration, Princeton, New Jersey, USA.
[3]Department of Atmospheric and Oceanic Sciences, University of California, Los Angeles, California, USA.

0886-6236/11/2011GB004059

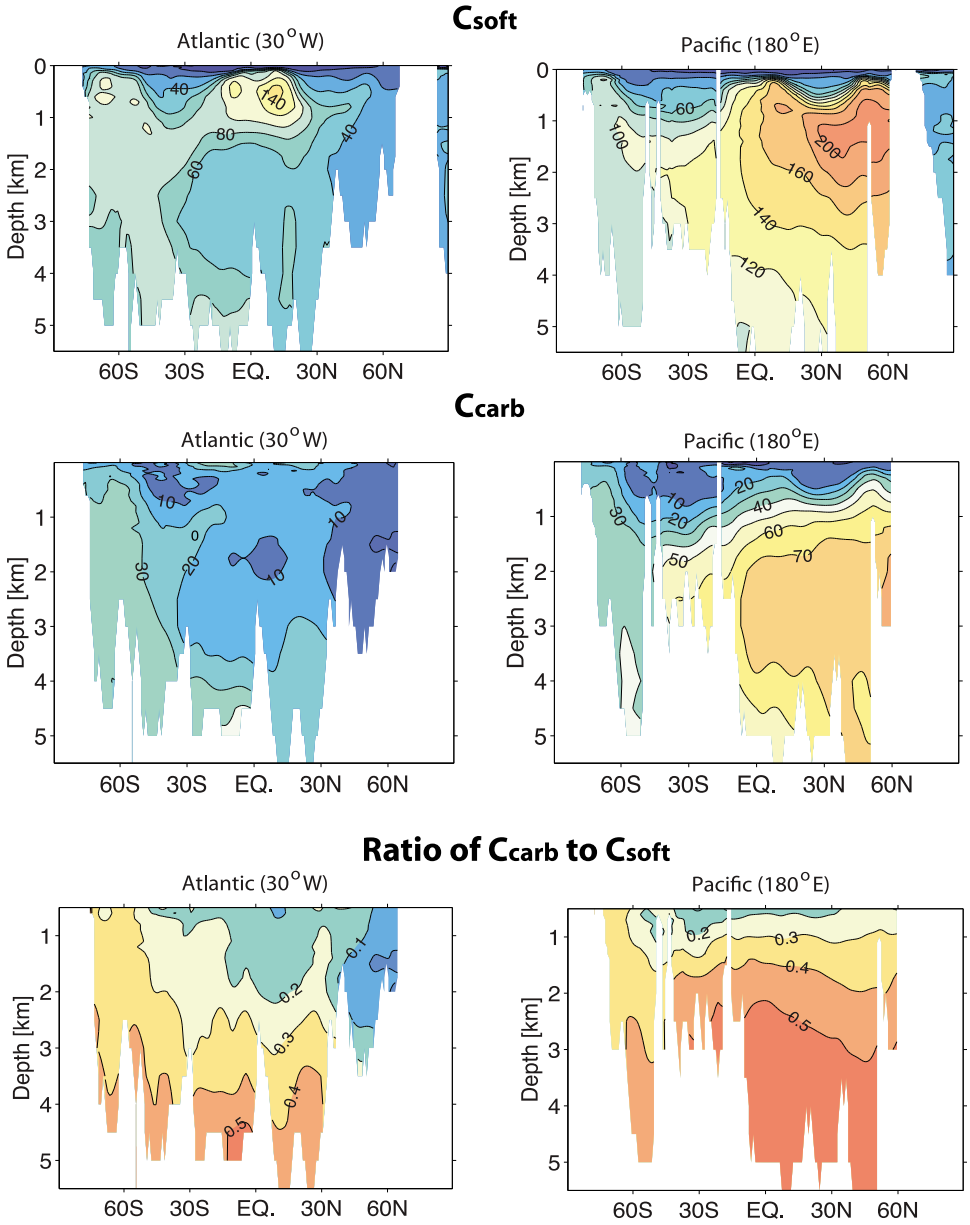

Figure 1. (top) The distribution of respired carbon as estimated from the Apparent Oxygen Utilization data [*Garcia et al.*, 2006] and a constant stoichiometric ratio of C: $-O_2$ = 117:170 [*Anderson and Sarmiento*, 1994]. (middle) The distribution of dissolved carbonate as estimated from the alkalinity data [*Key et al.*, 2004]. (bottom) The ratio of dissolved carbonate to respired carbon. Units for the top and middle panels are μmol kg^{-1}. The distributions of C_{soft} and C_{carb} are estimated following the approaches introduced by *Ito and Follows* [2005] and *Chung et al.* [2003] (See Appendix A). Cross sections along the (left) Atlantic (30°W) and (right) Pacific (180°E) are presented.

formation region. Surface biological consumption along this pathway utilizes most of the carbon and transports it back to depth. The second pathway can be characterized as a circuit involving the southward flow that feeds into the Antarctic Bottom Water (AABW) formation regions. Surface biological consumption in this pathway is inefficient, thus a substantial fraction of the upwelled biogenic carbon leaks out of the ocean into the atmosphere. The efficiency of carbon sequestration by the biological pump is thus set to a large degree by the pattern and strength of the global ocean ventilation [*Toggweiler et al.*, 2003; *Marinov et al.*, 2008]: changes in the partitioning of water between NADW and AABW, as well as changes in the absolute rate of overturning, have the potential to influence the ocean's storage of biogenic carbon and atmospheric pCO_2.

[4] The Southern Ocean ventilation rate has been linked to the glacial-interglacial change in atmospheric pCO_2 [e.g., *Sigman et al.*, 2010]. Paleoclimate proxy records indicate that the ventilation rate of the Southern Ocean was lower during glacial times and higher during interglacial times, exhibiting a significant correlation with the past atmospheric pCO_2 fluctuations [*François et al.*, 1997; *Marchitto et al.*,

2007; *Ahn and Brook*, 2008; *Anderson et al.*, 2009; *Sigman et al.*, 2010; *Skinner et al.*, 2010]. Modeling studies demonstrate that reduced rates of Southern Ocean overturning result in lowered atmospheric pCO_2 by effectively trapping respired carbon in the deep ocean [*Knox and McElroy*, 1984; *Sarmiento and Toggweiler*, 1984; *Siegenthaler and Wenk*, 1984; *Toggweiler*, 1999; *Ito and Follows*, 2005; *Toggweiler et al.*, 2006; *Marinov et al.*, 2008; *Hain et al.*, 2010]. However, a recent study [*Hain et al.*, 2010] made an important point that atmospheric pCO_2 responds only moderately to Southern Ocean stratification, since stratification sequesters both respired carbon and dissolved carbonate in the deep ocean. A sequestration of dissolved carbonate tends to counter the impact of a sequestration of respired carbon on atmospheric pCO_2 due to its influence on the alkalinity distribution [e.g., *Volk and Hoffert*, 1985; *Cermeño et al.*, 2008]. *Hain et al.* [2010] suggested that due partly to the counteracting effect, a reduction of Southern Ocean ventilation alone could only account for about a half of the reduction in atmospheric pCO_2 that occurred during the ice ages.

[5] The goal of this paper is to elucidate how changes in the global ocean circulation influence atmospheric pCO_2 through their influence on the oceanic storage of respired carbon and dissolved carbonate on millennial time scales. To this end, we develop a simple analytical framework relating changes in atmospheric pCO_2 to changes in the oceanic storage of biogenic carbon, in a closed system where the inventories of carbon and alkalinity are held constant in the ocean-atmosphere system. Our analytical framework builds upon the previous studies of *Ito and Follows* [2005] and *Marinov et al.* [2008] in which atmospheric pCO_2 is related to the oceanic storage of respired carbon in the limit of fast gas exchange. Our derivation extends the previously suggested relationship to include the strength of the carbonate pump, an approach similar to the study of *Goodwin et al*. [2008]. We apply this analytical framework to a suite of circulation models generated from an ocean general circulation model [*DeVries and Primeau*, 2009] to quantify the relative contributions from dissolved carbonate and respired carbon to the control of atmospheric pCO_2 by ocean circulation change.

[6] The circulation models used in this study span a wide range of overturning rates, water-mass distributions and ventilation ages. Based on our analysis of the models, we find the following: 1) The response of atmospheric pCO_2 to ocean circulation change is smaller than it would otherwise be because 13–39% of the change in atmospheric pCO_2 caused by a change in the oceanic storage of respired carbon is countered by a change in the storage of dissolved carbonate, a finding in accord with *Hain et al*. [2010]. 2) The air-sea carbon partitioning is primarily controlled by the Southern Ocean overturning rate, a finding consistent with previous studies [e.g., *Marinov et al.*, 2008]. However, the Southern Ocean control of atmospheric pCO_2 is greatly modulated by the overturning rate of NADW and the way surface productivity responds to circulation changes. The largest reduction in atmospheric pCO_2 of 44–88 ppm occurs in a model where reduced ventilation rates of both NADW and AABW cause the ocean to more effectively trap respired carbon within its interior. The uncertainty of a factor of two arises due to uncertainty in how surface productivity responds to circulation change. We discuss the implication of our findings for the glacial reduction in atmospheric pCO_2 in section 5.

2. A Simple Framework Relating the Strength of the Biological Pump to Atmospheric pCO_2

[7] We derive a simple analytical equation that relates atmospheric pCO_2 to the globally-averaged concentrations of respired carbon ($\overline{C_{soft}}$) and dissolved carbonate ($\overline{C_{carb}}$) in the ocean. A change in atmospheric pCO_2 can be written as

$$\Delta pCO_2^{atm} = \Delta pCO_2^{atm}\big|_{Alk} + \Delta pCO_2^{atm}\big|_{DIC} \tag{1}$$

where $\Delta\, pCO_2^{atm}|_{Alk}$ denotes the pCO_2 change due to alkalinity change and $\Delta\, pCO_2^{atm}|_{DIC}$ denotes the pCO_2 change due to DIC change. Previous studies [*Ito and Follows*, 2005; *Marinov et al.*, 2008] derived a relationship between atmospheric pCO_2 and the amount of respired carbon in the absence of alkalinity changes (i.e. $\Delta\, pCO_2^{atm}|_{DIC}$ only). Here we add the dissolved carbonate contribution to the previous work. We start with the carbon budget where the total amount of carbon in the ocean-atmosphere system $\sum C$ is written as

$$\sum C = V_a pCO_2^{atm} + M_o\left(\overline{C_{soft}} + \overline{C_{carb}} + \overline{C_{sat}} + \overline{C_{diseq}}\right). \tag{2}$$

Here V_a is the mole volume of the atmosphere, pCO_2^{atm} is the atmospheric partial pressure of CO_2, and M_o is the mass of sea water. The overbar represents globally averaged values, and C_{soft} and C_{carb} denote carbon remineralized from sinking organic particles and carbon dissolved from sinking biogenic $CaCO_3$, respectively. C_{sat} is the carbon concentration in the ocean if the surface ocean were in equilibrium with atmospheric pCO_2, and C_{diseq} is the carbon concentration due to air-sea disequilibrium that is transported into the ocean's interior. Assuming that the total inventory of carbon is conserved, a perturbation in the carbon cycle can be represented as

$$V_a \Delta pCO_2^{atm} = -M_o\left(\Delta\overline{C_{soft}} + \Delta\overline{C_{carb}} + \Delta\overline{C_{sat}} + \Delta\overline{C_{diseq}}\right) \tag{3}$$

where Δ denotes a perturbation. In our analytical derivation, we ignore the air-sea disequilibrium effect by assuming that the ocean is in equilibrium with the atmosphere while a perturbation is made (i.e. $\Delta\,\overline{C_{diseq}} = 0$). The Revelle factor R_C, which relates a fractional change in atmospheric pCO_2 to a fractional change in surface concentration of DIC while alkalinity is held constant [*Takahashi et al.*, 1980], is approximated by

$$\frac{\Delta pCO_2^{atm}|_{DIC}}{pCO_2^{atm}} \approx R_C \frac{\Delta\overline{C_{sat}}}{\overline{C_{sat}}}. \tag{4}$$

Substituting equation (4) into (3), we obtain

$$\left(V_a + \frac{M_o\overline{C_{sat}}}{R_C \cdot pCO_2}\right)\Delta pCO_2^{atm}|_{DIC} = -M_o\left(\Delta\overline{C_{soft}} + \Delta\overline{C_{carb}}\right). \tag{5}$$

Because $\frac{M_o\overline{C_{sat}}}{R_C V_a p\mathrm{CO}_2} \gg 1$, we can approximate $V_a\left(1+\frac{M_o\overline{C_{sat}}}{R_C V_a p\mathrm{CO}_2}\right)$ as $\frac{M_o\overline{C_{sat}}}{R_C p\mathrm{CO}_2}$ [*Ito and Follows*, 2005].Then equation (5) becomes

$$\frac{\Delta p\mathrm{CO}_2^{atm}|_{DIC}}{p\mathrm{CO}_2^{atm}} = -\frac{R_C}{\overline{C_{sat}}}\left(\Delta\overline{C_{soft}} + \Delta\overline{C_{carb}}\right). \quad (6)$$

[8] Now we turn our attention to the alkalinity contribution to the air-sea carbon balance. The total amount of alkalinity ($\sum Alk$) can be divided into the preformed (Alk_{pref}) and regenerated (Alk_{reg}) components with the former defined as the alkalinity that is transported from the surface to the ocean's interior by ocean circulation and the latter defined as the alkalinity added to/removed from subsurface water by dissolution of $CaCO_3$ minerals and oxidation of nitrate [*Brewer et al.*, 1975]

$$\sum Alk = M_o\left(\overline{Alk_{pref}} + \overline{Alk_{reg}}\right) = M_o\left(\overline{Alk_{pref}} + 2\overline{C_{carb}} - r_{N:C}\overline{C_{soft}}\right), \quad (7)$$

where $r_{N:C}$ is the stoichiometric ratio of nitrogen to carbon in organic matter. Assuming that the total inventory of alkalinity is conserved, we obtain that a perturbation of the biological pump can cause perturbations in other terms as

$$\Delta\overline{Alk_{pref}} = -2\Delta\overline{C_{carb}} + r_{N:C}\Delta\overline{C_{soft}}. \quad (8)$$

The Alkalinity factor R_A, which relates atmospheric $p\mathrm{CO}_2$ to surface alkalinity while DIC is held constant [*Takahashi et al.*, 1980], is approximated by

$$\frac{\Delta p\mathrm{CO}_2^{atm}|_{Alk}}{p\mathrm{CO}_2^{atm}} \approx R_A\frac{\Delta\overline{Alk_{pref}}}{\overline{Alk_{pref}}}. \quad (9)$$

Substituting equation (9) into (8), we obtain

$$\frac{\Delta p\mathrm{CO}_2^{atm}|_{Alk}}{p\mathrm{CO}_2^{atm}} = \frac{R_A}{\overline{Alk_{pref}}}\left(-2\Delta\overline{C_{carb}} + r_{N:C}\Delta\overline{C_{soft}}\right). \quad (10)$$

[9] Now we sum equations (6) and (10) to obtain

$$\frac{\Delta p\mathrm{CO}_2^{atm}}{p\mathrm{CO}_2^{atm}} = \Delta\overline{C_{soft}}\left(-\frac{R_C}{\overline{C_{sat}}} + r_{N:C}\frac{R_A}{\overline{Alk_{pref}}}\right) + \Delta\overline{C_{carb}}\left(-\frac{R_C}{\overline{C_{sat}}} - 2\frac{R_A}{\overline{Alk_{pref}}}\right). \quad (11)$$

If we use the global mean values for $R_C = 10$ and $R_A = -9.4$ [*Sarmiento and Gruber*, 2006], $\overline{C_{sat}} = 2100$ μmol kg^{-1} and $\overline{Alk_{pref}} = 2300$ μmol kg^{-1} [*Key et al.*, 2004], and $r_{N:C} = 0.14$ [*Anderson and Sarmiento*, 1994], equation (11) becomes

$$\frac{\Delta p\mathrm{CO}_2^{atm}}{p\mathrm{CO}_2^{atm}} = -0.0053\Delta\overline{C_{soft}} + 0.0034\Delta\overline{C_{carb}}. \quad (12)$$

Equation (12) shows the opposing effects of the soft-tissue and carbonate pumps on atmospheric $p\mathrm{CO}_2$. For example, an increase in respired carbon of 10 μmol kg^{-1} leads to a 5.3% decrease in atmospheric $p\mathrm{CO}_2$ whereas an increase in dissolved carbonate of 10 μmol kg^{-1} leads to a 3.4% increase in atmospheric $p\mathrm{CO}_2$. We note that equation (12) is derived for the ocean-atmosphere system where seawater chemistry does not interact with sediments. Below, we validate the analytical equation against a 3-D numerical model.

3. 3-D Model and Methods

[10] We use an off-line ocean circulation model coupled with a simple biogeochemistry module to examine the steady-state response of the air-sea carbon partitioning to change in ocean circulation. The horizontal resolution of the model is 3.75° × 3.75°, and the vertical resolution increases from 50 m at the surface to 300 m near the bottom. The control model (see below) has been used for model optimization and sensitivity analyses by *Kwon and Primeau* [2006, 2008]. Thus we refer readers to the previous work for details of model structure and its comparison with observations. In this section, we briefly describe the circulation and biogeochemistry models, and derive novel metrics for diagnosing the control of the oceanic storage of respired carbon by ocean circulation change in a 3-D model framework.

3.1. Circulation Models

[11] A suite of circulation fields is generated from an ocean general circulation model by varying the vertical diffusivity, the intensity of surface winds, and the surface temperature and salinity that are used to force the ocean circulation. The control (CTL) model is identical to the model used by *Primeau* [2005], *Kwon and Primeau* [2006, 2008] and *Kwon et al.* [2009]. Six different circulation fields are taken from *DeVries and Primeau* [2009]. For the "KL" and "KH" models, the vertical diffusivity coefficient is reduced from 0.5 cm^{2}s^{-1} ("CTL" model) to 0.15 cm^{2}s^{-1} ("KL" model) and increased to 0.85 cm^2 s^{-1} ("KH" model). For the "WL" and "WH" models, the wind stress that drives the ocean circulation is halved globally ("WL" model) and doubled globally ("WH" model). In the "PS1" and "PS2" models, the ocean model is forced by the surface temperature and salinity fields that are reconstructed for the Last Glacial Maximum [*Paul and Schäfer-Neth*, 2003]. The "PS1" model uses the surface condition of "Experiment G0" in the work of *Paul and Schäfer-Neth* [2003], which is based on a reconstructed sea surface temperature (SST) field with sea surface salinity (SSS) assumed to be uniformly higher by 1.07 psu than the present-day salinity distribution. The "PS2" model uses the surface condition of "Experiment G3" in the work of *Paul and Schäfer-Neth* [2003], which is the same as the boundary condition in the PS1 model except that there is an imposed 1 psu salinity anomaly in the Weddell Sea. The circulation models are fully spun up to an equilibrium, and the annual mean velocity and eddy-diffusivity tensor fields are taken to the off-line ocean biogeochemistry model.

[12] The suite of circulation models produce a wide range of global ocean ventilation patterns (Table 1 and Figure 2). We define the overturning rate of AABW as the maximum value below a depth of 2 km in the counter clockwise stream function integrated globally. Likewise, the overturning rate of NADW is defined as the maximum value north of 40°N

Table 1. Ventilation Characteristics Across the Circulation Models

Model[b]	Overturning Rate[a] (Sv)		Volume Fraction (%)			Ventilation Age (years)	
	AABW	NADW	AABW	NADW	Low Lat.	Southern Deep Water[c]	Global
KL	5	13	39	44	17	1720	1530
PS1	5	25	27	59	14	670	680
WL	11	13	65	20	15	460	640
CTL	11	15	62	21	17	430	590
WH	12	23	57	23	20	390	480
PS2	18	14	70	15	15	330	520
KH	19	16	70	14	16	210	370

[a]1 Sv = 10^6 m^3 s^{-1}.
[b]The models are arranged from top to bottom in order of increasing AABW overturning rate. "KL" = reduced vertical diffusivity, "KH" = increased vertical diffusivity. "WL" = reduced surface wind stress, "WH" = increased surface wind stress. "PS1" = Paul & Schäfer-Neth SST and SSS, "PS2" = saltier AABW than "PS1".
[c]Average of the ventilation age south of 40°S below a depth of 3000 m.

in the clockwise stream function integrated zonally for the Atlantic basin. The volume fractions of AABW and NADW in the global ocean are computed using a Green's function approach [*Primeau*, 2005], by assuming that the water masses formed south of 50°S correspond to AABW and the water masses formed north of 40°N in the Atlantic correspond to NADW. The ventilation age of the ocean is defined as the time that has elapsed since the water was last at the surface. We compute the ventilation age using a radiocarbon-like age tracer that has a uniform source at the surface and decays with an *e*-folding timescale of 8267 years. The preformed component (i.e. the age of water at the surface) is removed from the apparent radiocarbon age. As shown in Figure 2, the Southern Ocean overturning rate ranges from 5 Sv in the KL and PS1 models to 19 Sv in the KH model. The associated ventilation age of the Southern Ocean deep water is 1720 yr in the KL model, 670 yr in the PS1 model and 210 yr in the KH model.

3.2. Ocean Biogeochemistry Model

[13] The circulation fields are coupled with a simple biogeochemistry module [*Kwon et al.*, 2009], which is based on the second phase of the Ocean Carbon-cycle Model Intercomparison Project (OCMIP-II) [*Najjar et al.*, 2007]. In the OCMIP-II model, surface net community production is simulated by restoring simulated surface phosphate towards observed phosphate with a restoring time scale of 30 days whenever the model phosphate exceeds observations. Of the total organic carbon produced at the surface, 26% is exported as particulate organic matter whereas 74% is recycled in the upper ocean as dissolved organic matter. The organic particles exported from the euphotic zone (upper 75 m) become instantaneously remineralized back to inorganic matter with an attenuation profile following a power law curve with an exponent of −0.97 [*Martin et al.*, 1987]. The ratio of $CaCO_3$ to particulate organic carbon exported from the euphotic layer is set to 0.08 and the sinking $CaCO_3$ particles dissolve with an *e*-folding length scale of 2100 m. The stoichiometric ratio of C:N:P is 137:16:1 in the model [*Kwon and Primeau*, 2008].

[14] There is no sedimentation of organic carbon and $CaCO_3$ in this model, although potential feedbacks from bottom water-sediment interactions are discussed in section 5. A one-box model of the atmosphere is coupled with the ocean biogeochemistry model to conserve the total inventory of carbon in the ocean-atmosphere system, which is fixed at a value obtained from the CTL model throughout all the simulations. We discuss the uncertainty associated with the use of the OCMIP-II nutrient restoring model in section 4.3.

3.3. Diagnostics for the Change in the Oceanic Storage of Respired Carbon

[15] Changes in ocean circulation influence the oceanic storage of respired carbon through the following two mechanisms: 1) repartitioning of the global domain between the biologically efficient overturning circuit of NADW (with low preformed PO_4 concentration) and the inefficient overturning circuit of AABW (with high preformed PO_4 concentration), and 2) change in surface PO_4 distributions caused by changes in the rate at which nutrients are supplied to the surface and consumed by biology [*Toggweiler et al.*, 2003; *Marinov et al.*, 2008; *Schmittner and Galbraith*, 2008]. The first mechanism can be separated from the second if one assumes a hypothetical situation where the surface concentrations of PO_4 remain fixed at control values while the circulation change is made. In this section, we describe the separation method.

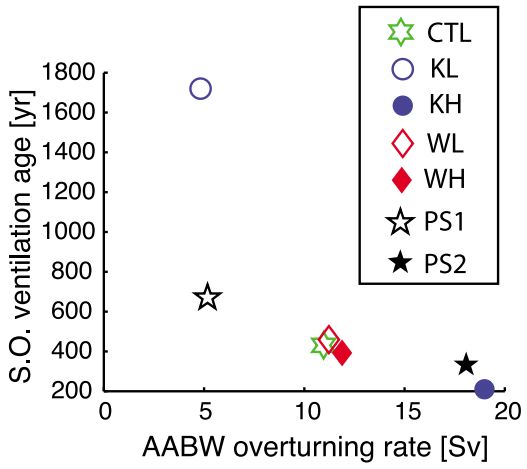

Figure 2. Southern Ocean ventilation characteristics across the circulation models as diagnosed with the AABW overturning rate and the ventilation age. See text for descriptions of the circulation models and the ventilation diagnostics.

[16] A change in the oceanic inventory of respired carbon scales linearly with a change in the global inventory of respired phosphate such that

$$\Delta\overline{C_{soft}} = r_{C:P}\Delta\overline{[PO_4]_{rem}} \tag{13}$$

where $r_{C:P}$ is a stoichiometric ratio of carbon to phosphorus and $[PO_4]_{rem}$ is phosphate remineralized from organic matter. When the total inventory of phosphate in the global ocean is conserved, a change in remineralized phosphate is mirrored by a change in preformed phosphate [*Ito and Follows*, 2005; *Marinov et al.*, 2008], therefore equation (13) becomes

$$\Delta\overline{C_{soft}} = -r_{C:P}\Delta\overline{[PO_4]_{pref}}. \tag{14}$$

[17] The globally averaged concentration of preformed PO_4 can be calculated by

$$\overline{[PO_4]_{pref}} = \frac{1}{M_o}\int_\Omega PO_4(r_s)\cdot G(r_s)d^2r_s \tag{15}$$

where the inventory of preformed PO_4 is obtained by integrating the convolution of surface PO_4, PO_4 (r_s), and the volume integrated Green's function, $G(r_s)$, over the entire surface ocean Ω [*Kwon et al.*, 2009; *Primeau*, 2005]. $G(r_s)$ denotes the volume of the ocean per unit surface area ventilated from the surface grid point, r_s, and characterizes the strength and pattern of the global ocean ventilation.

[18] From equation (15), $\overline{[PO_4]_{pref}}$ for the CTL model can be written as

$$\overline{[PO_4]^{CTL}_{pref}} = \frac{1}{M_o}\int_\Omega PO_4(r_s)^{CTL}\cdot G(r_s)^{CTL}d^2r_s, \tag{16}$$

which uses the surface PO_4 and Green's function obtained from the CTL model. Likewise, $\overline{[PO_4]_{pref}}$ for any other circulation model can be written as

$$\overline{[PO_4]^{m}_{pref}} = \frac{1}{M_o}\int_\Omega PO_4(r_s)^{m}\cdot G(r_s)^{m}d^2r_s, \tag{17}$$

where m could be KL, KH, WL, WH, PS1 and PS2.

[19] Now we subtract equation (16) from (17) to obtain

$$\begin{aligned}\overline{[PO_4]^{m}_{pref}} - \overline{[PO_4]^{CTL}_{pref}} = {} & \frac{1}{M_o}\int_\Omega PO_4(r_s)^{CTL}\cdot\left(G(r_s)^{m} - G(r_s)^{CTL}\right)d^2r_s \\ & + \frac{1}{M_o}\int_\Omega\left(PO_4(r_s)^{m} - PO_4(r_s)^{CTL}\right) \\ & \cdot G(r_s)^{m}d^2r_s.\end{aligned} \tag{18}$$

The first term on the right hand side is interpreted as the change in preformed PO_4 that would occur if the surface concentrations of PO_4 remained fixed at the control values while the ocean circulation changed. The second term, which is the difference between the net change on the left hand side and the first term on the right hand side, represents the change in preformed PO_4 associated with the redistribution of surface PO_4 in the model m.

[20] Substituting equation (18) in (14), we obtain

$$\begin{aligned}\Delta\overline{C_{soft}} = \overline{C^{m}_{soft}} - \overline{C^{CTL}_{soft}} = {} & -\frac{r_{C:P}}{M_o}\int_\Omega PO_4(r_s)^{CTL} \\ & \cdot\left(G(r_s)^{m} - G(r_s)^{CTL}\right)d^2r_s \\ & -\frac{r_{C:P}}{M_o}\int_\Omega\left(PO_4(r_s)^{m} - PO_4(r_s)^{CTL}\right) \\ & \cdot G(r_s)^{m}d^2r_s.\end{aligned} \tag{19}$$

The first term on the right hand side is the change in respired carbon that would occur if the circulation change were not accompanied by a change in nutrient concentrations at the surface. The second term is the change due to the redistribution of surface nutrients, which is controlled by ocean transport and surface biology.

4. Results and Discussions

4.1. The Control of Oceanic Storage of Biogenic Carbon by Circulation Change

[21] The inventories of respired carbon (C_{soft}) and dissolved carbonate (C_{carb}) vary widely across the models (Figure 3). Unlike the observation-based estimates (see Appendix A), the model-based estimates of C_{soft} and C_{carb} are precisely calculated by subtracting the preformed PO_4 and alkalinity (equation (15)) from the total concentrations, and by taking into account the stoichiometric ratios of C:N:P. The global inventories of C_{soft} and C_{carb} are 80–134 μmol kg^{-1} and 24–51 μmol kg^{-1}, respectively, across the circulation models. The ratio of respired carbon to dissolved carbonate stored in the ocean is roughly constant across the circulation models with a ratio of $\overline{C_{carb}}/\overline{C_{soft}}$ = 0.3–0.4 (Figure 3a).

[22] Consistent with previous studies [*Ito and Follows*, 2005; *Marinov et al.*, 2008], we find a good correlation between the oceanic storage of C_{soft} and the overturning rate of AABW (Figure 3b). The influence of the overturning rate of AABW on the oceanic storage of respired carbon mainly comes through the change in the partitioning of the global ocean domain between NADW and AABW (Figure 3c). A decreased overturning rate of AABW is generally accompanied by a decrease in the volume fraction of the global ocean that is ventilated from the Southern Ocean, which leads to a smaller fraction of respired carbon leaking out of the ocean [*Toggweiler et al.*, 2003; *Marinov et al.*, 2008; *Schmittner and Galbraith*, 2008]. In addition, changes in the overturning rates of AABW and NADW influence the rate at which respired carbon in the deep ocean is returned to the surface. In areas where the biological utilization rate is not fast enough to consume the respired carbon supplied to the surface, changes in the supply rate alter the concentrations of surface nutrients and hence the oceanic storage of respired carbon. For example, the increased overturning rate of NADW in the PS1 model (Table 1) elevates surface PO_4 concentrations, particularly north of 50°S (Figure 5e), while allowing respired carbon to leak out of the ocean (Figure 4). On the other hand, the reduced overturning rates of both AABW and NADW in the KL model (Table 1) help the global ocean to effectively store respired carbon (Figure 4), as reflected by the decreased concentrations of surface and preformed PO_4 (Figure 5c).

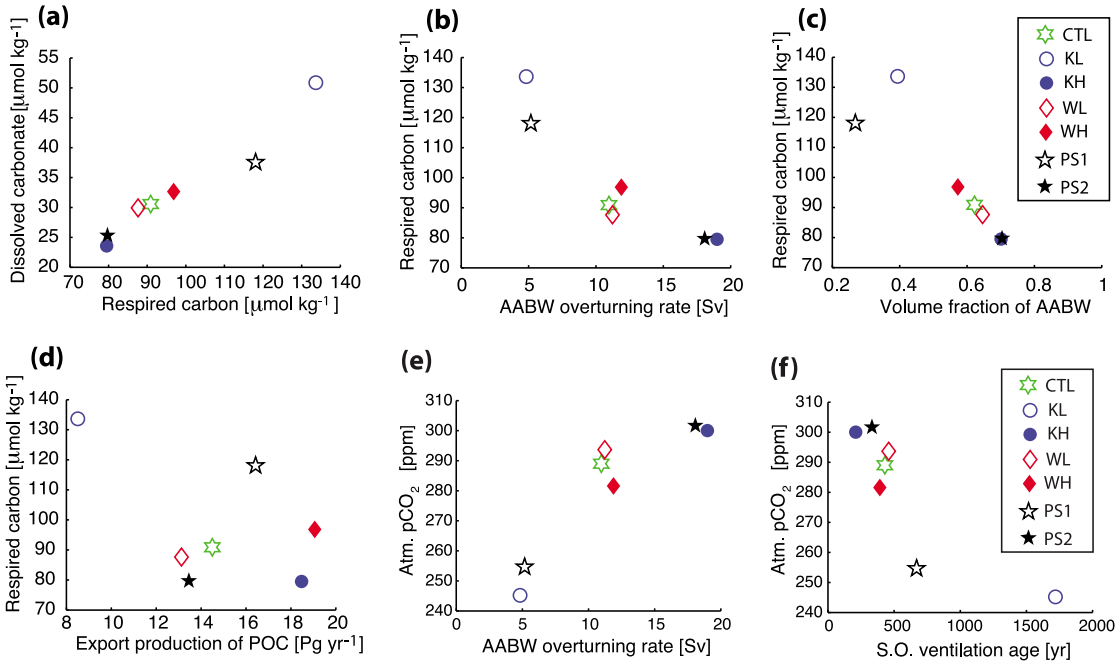

Figure 3. (a) The globally averaged concentrations of respired carbon and dissolved carbonate, estimated from the circulation models. (b-d) Globally averaged concentration of respired carbon as a function of the AABW overturning rate, the volume fraction of the global ocean ventilated from the Southern Ocean, and the globally integrated export production of particulate organic carbon at the base of the euphotic layer. (e-f) Atmospheric pCO_2 obtained from the "Fgasx + Csolu" run as a function of the AABW overturning rate and the ventilation age of Southern Ocean deep water.

[23] Under steady-state conditions, export production is a poor indicator of the oceanic storage of respired carbon (Figure 3d) [*Marinov et al.*, 2008; *Kwon et al.*, 2009]. For example, the oceanic storage of respired carbon increases from 91 μmol kg^{-1} (CTL model) to 134 μmol kg^{-1} in the KL model despite the fact that the globally integrated export production of particulate organic carbon decreases from 14.5 Pg yr^{-1} to 8.5 Pg yr^{-1}. This is because the residence

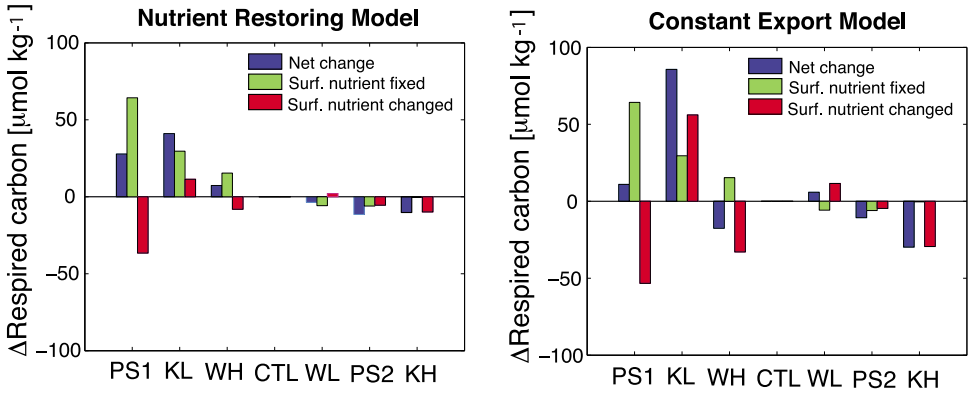

Figure 4. Changes in the oceanic storage of respired carbon relative to the CTL model. The blue bar represents the net change in respired carbon from the CTL model to each model. The green bar represents the change that would occur if the concentrations of surface nutrients remained fixed at the CTL values when the ocean circulation changed from the CTL to each model. This term can be expressed as $-\frac{r_{C:P}}{M_o}\int_\Omega PO_4\ (r_s)^{CTL} \cdot (G(r_s)^m - G(r_s)^{CTL})\ d^2r_s$ (see section 3.3). The red bar is the difference between the blue bar and the green bar, and represents the change in the oceanic storage of respired carbon associated with changes in surface nutrient distributions from the CTL model to each model. This term can be expressed as $-\frac{r_{C:P}}{M_o}\int_\Omega (PO_4\ (r_s)^m - PO_4\ (r_s)^{CTL}) \cdot G(r_s)^m\ d^2r_s$. Results from the nutrient restoring and constant export models are presented. Note that the green bars (the hypothetical situation where surface PO_4 is fixed at the control value) remain the same between the nutrient restoring and constant export models. The circulation models are arranged from left to right in order of increasing volume fraction of the global ocean ventilated by AABW.

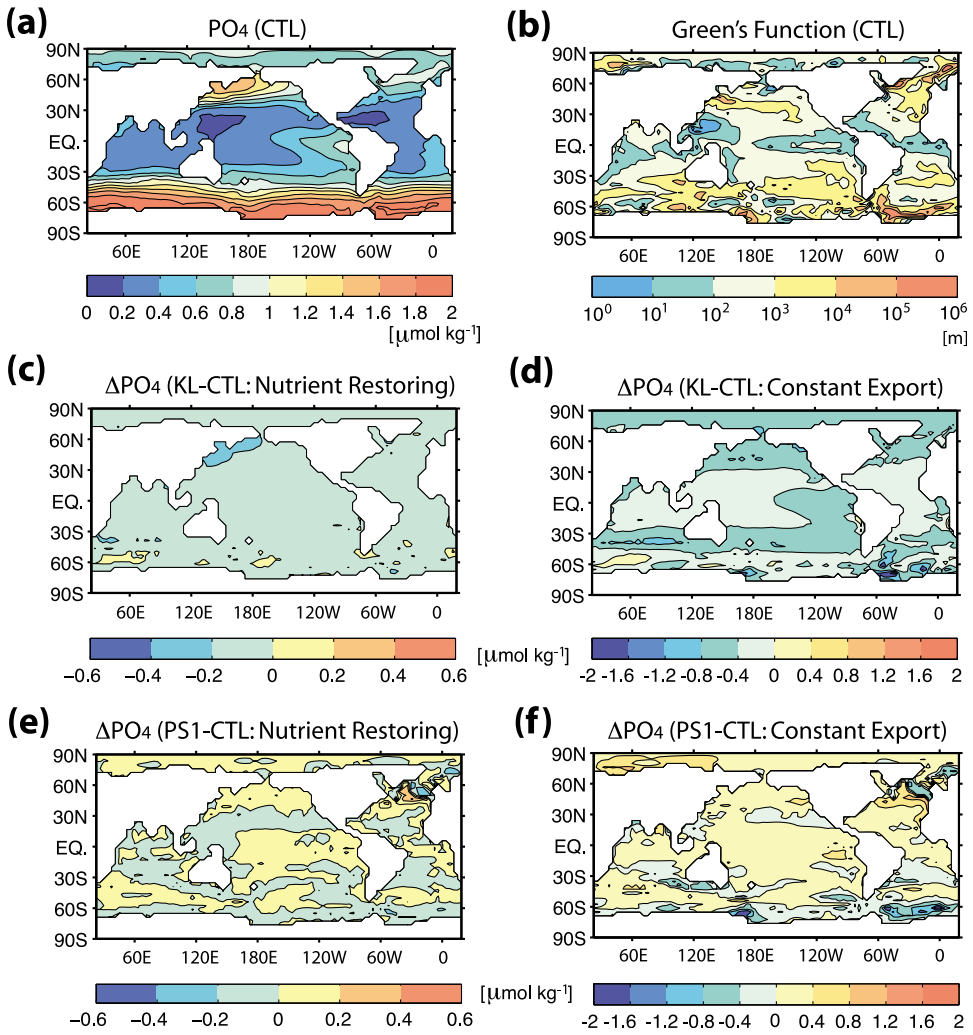

Figure 5. (a) The distribution of surface PO_4 in the CTL model in μmol kg^{-1}. (b) The Green's function for the CTL model representing the volume of the ocean ventilated from each surface grid divided by the area of the surface grid (unit is m). Note that the color scale is in the logarithmic scale. Redrawn from *DeVries and Primeau* [2009, Figure 2]. (c–d) Changes in surface PO_4 concentrations from the CTL model to KL model for the nutrient restoring and constant export models. (e–f) Changes in surface PO_4 concentrations from the CTL model to PS1 model. Units are μmol kg^{-1} for Figures 5c, 5d, 5e, and 5f. Note the different color scales between the nutrient restoring model and constant export model.

time of regenerated carbon in the deep ocean increases in the KL model, which tends to increase the inventory of respired carbon despite the reduced export production. On the other hand, an increased productivity in the PS1 model does contribute to an increase in the oceanic storage of respired carbon (see section 4.3 for a further discussion).

4.2. The Control of Atmospheric pCO_2 by Circulation Change

[24] In agreement with *Hain et al.* [2010], we find that the response of atmospheric pCO_2 to a change in ocean circulation is due not just to the response of respired carbon to the circulation change, but also to the counteracting effects of changes in the storage of dissolved carbonate. Here we demonstrate the counteracting effect using the analytical framework derived in section 2.

[25] Changes in ocean circulation influence atmospheric pCO_2 via three mechanisms in this model - the CO_2 solubility effect due to changes in temperature and salinity, the air-sea CO_2 disequilibrium effect associated with changes in the residence time of water at the surface, and changes in the oceanic storage of biogenic carbon. To suppress the effects of variations in temperature, salinity and air-sea CO_2 disequilibrium across the models, we perform a series of simulations: 1) The "Ngasx + Vsolu" run in which normal gas exchange coefficient is taken from the OCMIP-II model [*Najjar et al.*, 2007; *Wanninkhof*, 1992] and the effects of varying temperature and salinity are taken into account. 2) The "Fgasx + Vsolu" run in which the gas exchange coefficient used in the "Ngasx + Vsolu" run is increased by a factor of 10^5 in order to bring the sea-surface pCO_2 into equilibrium with the atmospheric pCO_2. 3) The "Fgasx +

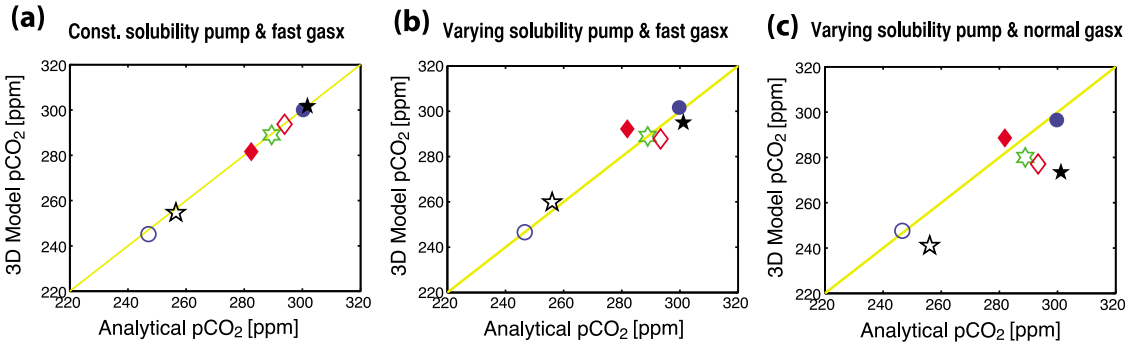

Figure 6. Comparison of analytical atmospheric pCO_2 obtained from equation (20), $pCO_2^{atm} = 420\exp(-0.0053\overline{C_{soft}} + 0.0034\overline{C_{carb}})$, with atmospheric pCO_2 obtained from the 3-D model simulations. (a) The "Fgasx + Csolu" run in which the air-sea carbon disequilibrium is suppressed and a constant solubility pump is imposed. (b) The "Fgasx + Vsolu" run in which the air-sea carbon disequilibrium is suppressed and the solubility pump is allowed to vary. (c) The "Ngasx + Vsolu" run in which the air-sea carbon disequilibrium effect is taken into account and the solubility pump is allowed to vary.

Csolu" run in which, in addition to the use of the fast gas exchange coefficient, a constant solubility pump is imposed across the circulation models by holding surface temperature and salinity fields constant at 3.8°C and 34.7 psu (of which the values are chosen such that the atmospheric pCO_2 and the oceanic inventory of carbon in the CTL model remain the same between the "Fgasx + Vsolu" and "Fgasx + Csolu" runs).

[26] Figure 6 compares the atmospheric pCO_2 obtained from the 3-D model with the pCO_2 obtained from the following equation:

$$pCO_2^{atm} = 420\exp\left(-0.0053\overline{C_{soft}} + 0.0034\overline{C_{carb}}\right) \qquad (20)$$

which is obtained from equation (12) using the control values of $\overline{C_{soft}} = 91\ \mu\text{mol kg}^{-1}$, $\overline{C_{carb}} = 31\ \mu\text{mol kg}^{-1}$ and $pCO_2^{atm} = 289$ ppm (taken from the CTL of the "Fgasx + Csolu" simulation). The root mean square error is less than 1 ppm when the "Fgasx + Csolu" run is compared with equation (20). This good agreement indicates that the sensitivity of atmospheric pCO_2 to change in the oceanic storage of biogenic carbon is largely set by the surface average values of Revelle and Alkalinity factors, an assumption made in our analytical derivation and suitable for small perturbations in the ocean-atmosphere carbonate system. With the solubility and disequilibrium effects turned on, the simulated atmospheric pCO_2 deviates further from the value predicted by the simple theory of equation (20). Although the CO_2 solubility pump and disequilibrium effects are important in modulating the control of atmospheric pCO_2 by circulation change, the oceanic storage of biogenic carbon is the dominant factor in explaining the spread of atmospheric pCO_2 across the circulation models (Figure 6). Thus we focus on the "Fgasx + Csolu" run only in the remainder of this paper.

[27] Now we use the analytical framework, equation (12), to diagnose the relative contributions from respired carbon and dissolved carbonate to the net change in atmospheric pCO_2 (Table 2). For all of the circulation fields examined in this study, changes in the respired carbon pool affect atmospheric pCO_2 more than changes in the dissolved carbonate pool, which tend to partially offset the soft-tissue pump-driven change in atmospheric pCO_2. The offset varies with the circulation, ranging from 13% to 39% (Table 2). One of the largest offsets (30%) occurs in the "KL" model where a −65 ppm decrease in atmospheric pCO_2 caused by an accumulation of respired carbon is countered by a 20 ppm increase due to a concomitant accumulation of dissolved

Table 2. Atmospheric pCO_2 Obtained From the Nutrient Restoring Model

	3-D Model[a]: pCO_2 ($\Delta\ pCO_2$) (ppm)			Theory[b]: $\Delta\ pCO_2$ (ppm)			
Model	Ngasx + Vsolu	Fgasx + Vsolu	Fgasx + Csolu	$\Delta\ pCO_2^{soft} + \Delta\ pCO_2^{carb}$	$\Delta\ pCO_2^{soft}$	$\Delta\ pCO_2^{carb}$	% Offset by Carbonate
KL	248 (−32)	248 (−42)	245 (−44)	−46	−66	20	−30
PS1	241 (−39)	261 (−29)	255 (−34)	−35	−42	7	−16
WL	277 (−3)	288 (−2)	294 (5)	4	5	−1	−13
CTL	280 (0)	289 (0)	289 (0)	0	0	0	-
WH	289 (9)	293 (4)	282 (−7)	−7	−9	2	−22
PS2	273 (−7)	296 (6)	302 (13)	12	17	−5	−30
KH	296 (16)	301 (12)	300 (11)	11	18	−7	−39

[a]The "Ngasx + Vsolu" run accounts for the effects of the redistribution of biogenic carbon, air-sea carbon disequilibrium and varying surface temperature and salinity when calculating atmospheric pCO_2. For the "Fgasx + Vsolu" run, the air-sea carbon disequilibrium effect is suppressed by increasing the gas exchange coefficient. For the "Fgasx + Csolu" run, we also suppress the solubility pump by imposing a constant solubility pump across models. ΔpCO_2 represents the relative change with respect to the CTL pCO_2.

[b]Analytical equation (12), $\Delta pCO_2 = \Delta pCO_2^{soft} + \Delta pCO_2^{carb} = pCO_2\,(-0.0053\Delta\overline{C_{soft}} + 0.0034\Delta\overline{C_{carb}})$, is used to obtain the net change in atmospheric pCO_2, contributions from respired carbon and dissolved carbonate, and the percentage offset by the carbonate pump.

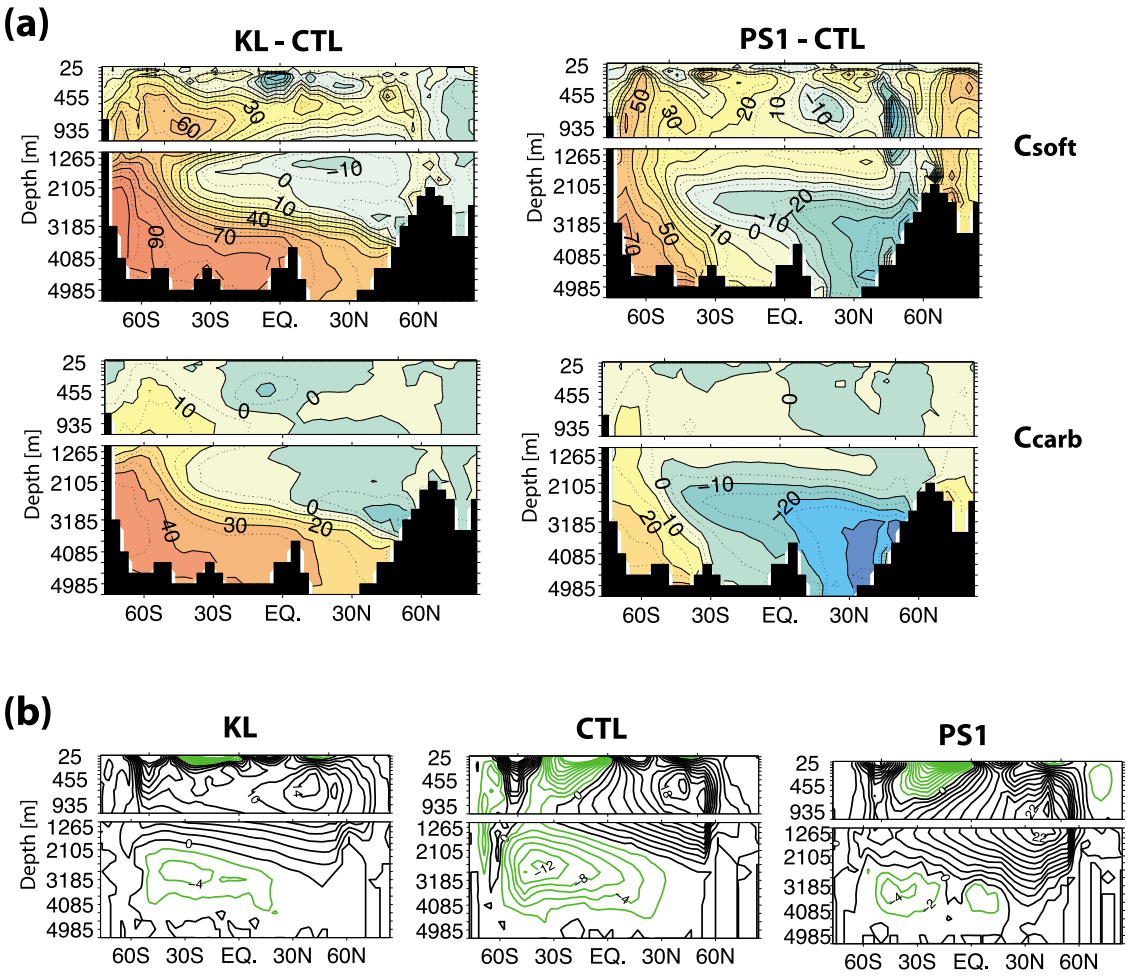

Figure 7. (a) (left) Differences between the KL and CTL models and (right) differences between the "PS1" and "CTL" models of the zonally averaged concentrations of (top) C_{soft} and (bottom) C_{carb} along the Atlantic. Units are μmol kg^{-1}. These are obtained from the nutrient restoring model. (b) The global stream functions in the "KL", "CTL" and "PS1" models. Contour interval of the stream function is 2 Sv (1 Sv = 10^6 m^3 s^{-1}). Black lines indicate clockwise circulation. Green lines indicate counter-clockwise circulation.

carbonate in the deep water. On the other hand, one of the smallest offsets (16%) occurs in the "PS1" model where the soft-tissue pump contribution of −41 ppm is countered by the carbonate pump contribution of 7 ppm. The larger offset occurs in the KL model because reduced overturning rates of southern and northern sourced deep waters make the C_{carb}-rich deep ocean poorly ventilated (Figure 7).

[28] Overall, we find that atmospheric pCO_2 is determined primarily by the overturning rate of AABW (Figures 3e and 3f) due to its ability to regulate the global inventories of preformed and regenerated nutrients. This is what one would expect from the relationship between the oceanic storage of biogenic carbon and the Southern Ocean overturning rate (Figure 3b) and the analytical framework presented in section 2.

4.3. Surface Productivity as a Modulator of the Southern Ocean Control of Atmospheric pCO_2

[29] An important source of uncertainty arises due to the model's assumption that surface community productivity depends on macro-nutrient supply by ocean circulation, an assumption intrinsic to the OCMIP-II nutrient restoring model. In parts of the ocean where new productivity is not limited by macro-nutrients (such as high nutrient, low chlorophyll regions), the surface community productivity will be insensitive to change in nutrient supply by ocean circulation, rendering the assumption inadequate. To examine the uncertainty associated with the nutrient restoring model, we performed a simulation where we held the net community production fixed at a value obtained from the CTL model as long as surface phosphate does not fall below zero. When the surface phosphate concentration falls below zero, the surface production is turned off [*Kwon et al.*, 2009]. This constant export model provides the other end of the spectrum in which the global surface productivity is assumed to be limited by external forcing such as light or micro-nutrients from the atmosphere [*Sarmiento et al.*, 1998].

[30] We find that the simulated atmospheric pCO_2 is very sensitive to the way surface productivity responds to circulation change (Figure 8). The constant export model amplifies

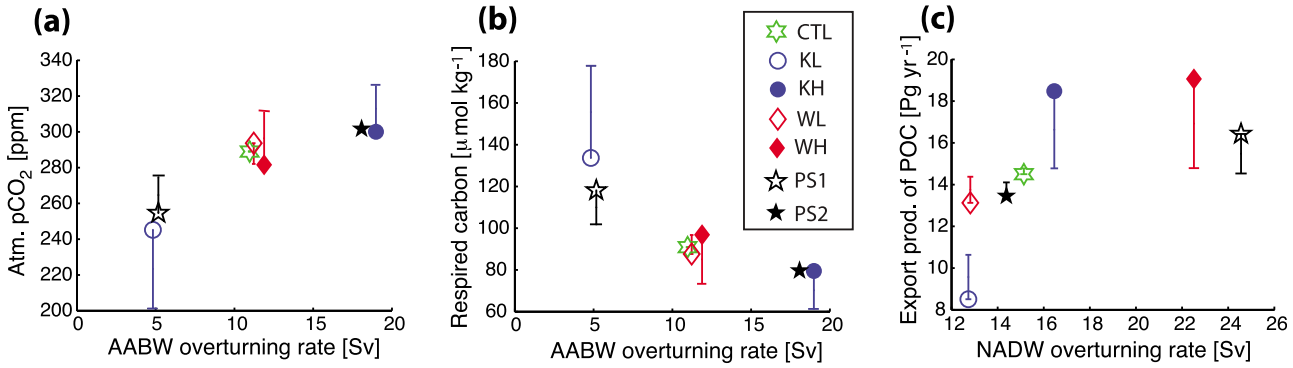

Figure 8. (a) Atmospheric pCO_2 as a function of AABW overturning rate, same as Figure 3e except that error bars are drawn based on the simulations with the constant export model. (b) The globally averaged concentration of respired carbon as a function of AABW overturning rate. (c) Globally integrated export production of particulate organic carbon as a function of NADW overturning rate. One end of each error bar (as marked by symbols) represents the nutrient restoring model where surface community productivity is assumed to be very sensitive to change in macro-nutrient supply by ocean circulation. The other end of error bar represents the constant export model where surface productivity is assumed to be insensitive to change in nutrient supply by ocean circulation.

the change in atmospheric pCO_2 driven by ocean circulation change in the KL model: atmospheric pCO_2 drops by 88 ppm, twice as much as the pCO_2 reduction obtained in the nutrient restoring model. This is largely due to the fact that the inventory of respired carbon increases by 87 μmol kg^{-1} in the constant export model, twice as much as the increase of 43 μmol kg^{-1} in the nutrient restoring model (Figure 4). This is in turn caused by the reduced overturning rates of the northern and southern sourced waters that accompany a minimal reduction of export production of particulate organic carbon (a reduction of only 4 PgC/yr in the constant export model compared with a reduction of 6 PgC/yr in the nutrient restoring model). The additional increase in respired carbon of 44 μmol kg^{-1} in the constant export model is thus due to the additional export production of 2 PgC/yr that is effectively stored in the poorly ventilated deep waters in the KL model. In other words, the constant export model allows the reduced ventilation rates of the northern and southern sourced deep water to reduce the surface concentrations of PO_4 more than does the nutrient restoring model (Figure 5). The greater reduction of preformed PO_4 in the constant export model is associated with a greater increase in respired carbon stored in the ocean, which results from more efficient utilization of PO_4 by surface biology.

[31] On the other hand, the constant export model dampens the response of atmospheric pCO_2 to ocean circulation change in the PS1 model: atmospheric pCO_2 drops by only 14 ppm in the constant export model compared to a 34 ppm reduction in the nutrient restoring model. In the PS1 model, the overturning rate of NADW increases from 15 Sv in the CTL model to 25 Sv. Accordingly, the upwelling rate of PO_4 increases in the PS1 model. This results in raising the export production of particulate organic carbon by 2 PgC/yr in the nutrient restoring model, whereas the export production remains constant at a value obtained from the CTL model in the constant export model (Figure 8c). The decreased export production of 2 PgC/yr in the constant export model (relative to the nutrient restoring model) leads to a decrease in the oceanic storage of respired carbon of 16 μmol kg^{-1} (Figure 4), which is mainly responsible for the smaller reduction in atmospheric pCO_2 in the constant export model.

4.4. NADW Ventilation as a Modulator of the Southern Ocean Control of Atmospheric pCO_2

[32] A comparison between the KL and PS1 models highlights an important role of the NADW overturning in modulating the Southern Ocean control of the air-sea carbon partitioning. The distinction can be made clearer when we consider the constant export model where a feedback from the surface productivity response to ocean circulation change is suppressed and hence changes in ventilation rates exert greater influence on surface nutrient concentrations. In both the KL and PS1 models, the overturning rate of AABW decreases from the control value of 11 Sv to 5 Sv, and the subsequent increase in the oceanic storage of biogenic carbon tends to reduce atmospheric pCO_2. However, the response of atmospheric pCO_2 differs greatly between the two models (−88 ppm vs. −14 ppm). In other words, the reduced ventilation rate of AABW has a greater impact on the oceanic storage of respired carbon in the KL model than in the PS1 model: an increase of 87 μmol kg^{-1} in the KL model compared to an increase of 11 μmol kg^{-1} in the PS1 model (Figure 4).

[33] This difference in sensitivity can be attributed to different ventilation patterns of NADW. A reduced overturning rate of NADW along with its increased ventilation age in the KL model tends to further increase the respired carbon stored in the ocean. On the other hand, the respired carbon trapped through the reduced ventilation rate of AABW in the PS1 model upwells to the surface through the enhanced NADW overturning circuit. A large portion of the increased amount of respired carbon that flows northward leaks out of the ocean, as indicated by increased concentrations of surface PO_4 in the NADW formation regions (Figure 5). This contrast between the KL and PS1 models is less pronounced in the nutrient restoring model where a portion of the upwelled respired carbon is returned to the

deep water through increased biological utilization at the surface in the PS1 model.

5. Implications for the Glacial Reduction in Atmospheric pCO_2

[34] Although it was not our goal to reproduce the ocean circulation pattern for the Last Glacial Maximum (LGM), the KL model (in comparison to the CTL model) has some interesting analogies to the LGM ocean circulation pattern inferred from paleoproxy records. Based on the radiocarbon content of surface- and bottom-dwelling organisms that are preserved in ocean sediments, *Skinner et al.* [2010] suggested that the Atlantic sector of the Southern Ocean was poorly ventilated during the LGM: the ventilation age increased by 1.6–3 times relative to the present-day, which is slightly lower than the increase in the ventilation age estimated from the KL model (a four-fold increase relative to the CTL model). Such a large increase in the ventilation age in the Southern Ocean deep water results from weakened overturning rates of the northern and southern sourced deep waters (Table 1). Additionally, reduced mixing across isopycnal surfaces (as imposed in the KL model) of the deep ocean has been invoked by recent modeling and observational studies [*Bouttes et al.*, 2010, 2011; *Lund et al.*, 2011] as an essential component that drives the observed carbon cycles and oxygen isotope distributions during the LGM. A detailed discussion of the biogeochemical evidence of the consistency of the KL model with paleoproxy observations will be reported elsewhere.

[35] Assuming that the KL model captures the gross features of the LGM ocean circulation, this study suggests that a considerable fraction (~30%) of the respired carbon driven change in atmospheric pCO_2 might be negated by the carbonate pump driven change when the ventilation rate of bottom water weakens, a finding consistent with *Hain et al.* [2010].

[36] The decrease in atmospheric pCO_2 of 44–88 ppm in the KL model is a consequence of reduced ventilation rates of the southern sourced deep water (55% reduction in the AABW overturning rate) and the northern sourced deep water (13% reduction in the NADW overturning rate), which cause the global ocean to effectively trap respired carbon within the ocean's interior. The increased amount of respired carbon, in turn, results from the increased residence time of respired carbon in the deep ocean. It is important to note that the oceanic storage of respired carbon increases in the KL model despite the fact that the amount of organic carbon exported from the surface decreases globally (Figure 8c).

[37] Although the mechanism by which the KL model draws down atmospheric pCO_2 is qualitatively consistent with the previous studies of *Hain et al.* [2010] and *Toggweiler* [1999], the atmospheric pCO_2 response to a reduced ventilation rate of the Southern Ocean differs quantitatively from previous studies. The 44–88 ppm reductions in the KL model can be compared with the 21 ppm reductions obtained by *Hain et al.* [2010] and *Toggweiler* [1999], the changes in atmospheric pCO_2 being attributed solely to the oceanic accumulation of biogenic carbon without the $CaCO_3$ compensation response (see below for a discussion). As discussed in this paper, three factors come into play in the quantitative assessment of the control of atmospheric pCO_2 by ocean ventilation change: 1) the counteracting effect of the accumulation of dissolved carbonate on the change in atmospheric pCO_2 driven by the storage of respired carbon, 2) the ventilation rates of the southern and northern sourced deep waters, which determine the residence time of the carbon respired from sinking organic particles within the ocean's interior, and 3) the surface productivity response to circulation change, which has a direct impact on the oceanic storage of biogenic carbon. The interplay between the latter two factors controls surface nutrient concentrations and the global preformed nutrients.

[38] The large sensitivity of atmospheric pCO_2 to ocean ventilation change in this study, compared to previous box model studies [*Hain et al.*, 2010; *Toggweiler*, 1999], is thought to be largely due to different assumptions about how biological productivity responds to ocean circulation changes (Daniel Sigman and Mathis Hain, personal communications). We find that the response in surface nutrient concentrations to ocean ventilation change is greater in the KL model than the values assumed by *Hain et al.* [2010] and *Toggweiler* [1999]. This is particularly the case over the deep water formation regions of the northern North Atlantic and the Southern Ocean (Figure 5). The concentrations of surface PO_4 drop by as much as 30–100% over the Weddell Sea, a highly localized area where AABW forms in the KL model, in response to a reduced ventilation rate of AABW. Importantly, surface PO_4 concentrations over the NADW formation region also drop substantially in response to a reduced ventilation rate of NADW in both nutrient restoring and constant export models. The large decrease in surface PO_4 in the NADW formation region results from the combined effect of the downward shift of nutrients (Figure 7) and the return pathway of the upwelled circumpolar deep water into the NADW formation region. The northward flow of Antarctic Intermediate Water and Subantarctic Mode Water transfers the waters depleted in PO_4 to the NADW formation region with surface PO_4 being increasingly depleted towards the subpolar gyre [*Kwon et al.*, 2009]. This effect is even greater in the constant export model where surface nutrients are effectively transformed into respired carbon by the biological pump, further depleting PO_4 in the upper ocean. Compared to the downwelling regions, the change in surface PO_4 is far less in regions where deep waters upwell into the surface (Figure 5). This heterogeneous response of surface nutrient concentrations to circulation change raises a great challenge to any effort to measure the glacial utilization of surface PO_4 as an attempt to unravel the oceanic role in the glacial reduction in atmospheric pCO_2 [e.g., *Robinson and Sigman*, 2008].

[39] On timescales relevant to the glacial-interglacial climate cycles, an important feedback comes through the open system response where bottom water chemistry interacts with $CaCO_3$ sediments [*Broecker and Peng*, 1987; *Boyle*, 1988; *Archer and Maier-Reimer*, 1994; *Archer et al.*, 2000; *Sigman and Boyle*, 2000; *Toggweiler*, 1999; *Chikamoto et al.*, 2008]. Accumulation of respired carbon will make bottom waters more corrosive to $CaCO_3$ sediments. This will drive more dissolution of $CaCO_3$ sediments until the burial fluxes of $CaCO_3$ balance the dissolution fluxes and the river inputs from terrestrial weathering. A more alkaline ocean will draw more CO_2 out of the atmosphere. We infer a potential feedback from $CaCO_3$ sediments by calculating the saturation state (Δ CO_3) of sea water with respect to calcite minerals

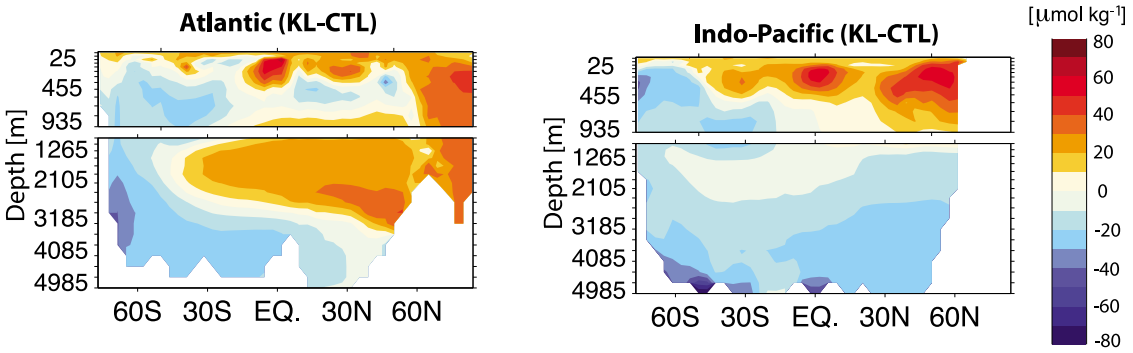

Figure 9. Change in the saturation state ($\Delta\Delta CO_3 = \Delta CO_3^{insitu} - \Delta CO_3^{sat}$) from the CTL model to KL model. The saturation state (ΔCO_3) is obtained by taking a difference between in-situ carbonate ion concentration (CO_3^{insitu}) and saturation carbonate ion concentration (CO_3^{sat}), which is a function of temperature, salinity and pressure. The zonally averaged fields are presented for the (left) Atlantic and (right) Indo-Pacific. Units are μmol kg^{-1}. Positive values represent increases in the saturation state of sea water with respect to $CaCO_3$ minerals whereas negative values represent decreases in the saturation state.

[*Zeebe and Wolf-Gladrow*, 2009]. We find that the saturation state of bottom waters decreases globally in the KL model, making bottom waters more corrosive to $CaCO_3$ sediments (Figure 9). This implies that the $CaCO_3$ compensation response in the KL model is likely to amplify the closed system response in atmospheric pCO_2 of 44–88 ppm.

[40] Quantitative assessments of circulation change and the associated carbon cycle response that might have occurred during the ice ages still remain an area of active research. A more thorough investigation should take into account the terrestrial carbon cycling, changes in temperature and salinity, and interactions between the ocean and sea ice with a quantitative assessment of model uncertainties. Nonetheless, this study highlights an important role for the overturning rate of NADW and the associated response of surface productivity to circulation change in modulating the impact of the Southern Ocean stratification on the air-sea carbon partitioning. This suggests that the hypothesis that invokes the Southern Ocean ventilation change as a driver of the glacial reduction in atmospheric pCO_2 should be expanded to include the ventilation change of the North Atlantic. We propose a revised hypothesis that a synchronously reduced ventilation rate of both *northern* and *southern* sourced deep waters could lead to the large glacial reduction in atmospheric pCO_2 of 80–100 ppm.

Appendix A

A1. Observational Constraint of Respired Carbon and Dissolved Carbonate

[41] Following *Ito and Follows* [2005], we estimate respired carbon (C_{soft}) by multiplying Apparent Oxygen Utilization (AOU) with a constant stoichiometric ratio of C: $-O_2 = 117 \pm 14{:}170 \pm 10$ [*Anderson and Sarmiento*, 1994]. Although this approach is prone to a large uncertainty associated with the assumption that the surface ocean is in equilibrium with the oxygen concentration in the atmosphere [*Ito et al.*, 2004], we believe that AOU gives a good approximation to the gross distribution of respired carbon. The globally averaged concentration of respired carbon is estimated to be 103 ± 20 μmol kg^{-1} where the $\pm$ range accounts for the uncertainty in the stoichiometric ratio.

[42] The basin-scale distribution of carbon dissolved from $CaCO_3$ (C_{carb}) was previously estimated by *Feely et al.* [2002], *Sabine et al.* [2002] and *Chung et al.* [2003]. Here we adopt the method from the previous studies to obtain the global-scale distribution of C_{carb} using the globally gridded data sets of alkalinity from the Global Ocean Data Analysis Project [*Key et al.*, 2004] and salinity, temperature, AOU and phosphate from the World Ocean Atlas [*Garcia et al.*, 2006]. We use the following relationship [*Chung et al.*, 2003] to infer C_{carb} from alkalinity and AOU:

$$C_{carb} = 0.5\left(Alk - Alk_{pref}\right) + 0.63(0.0941 \times \mathrm{AOU}) \qquad \text{(A1)}$$

where Alk_{pref} is the preformed alkalinity and the second term on the right hand side accounts for the contribution from the oxidation of organic nitrogen, phosphorus and sulfur to alkalinity distribution [*Kanamori and Ikegami*, 1982; *Chung et al.*, 2003]. The factor of 0.5 reflects the fact that addition of one mole of dissolved carbonate increases alkalinity by two moles. We estimate Alk_{pref} using a multi-linear regression model constructed based on conservative tracers of salinity (S), potential temperature (pT), and PO ($PO = O_2 - r_{O2:P} \times PO_4$) in which $r_{O2:P}$ is the stoichiometric ratio of O_2 to phosphorus. The resulting regression model for the global ocean is

$$Alk_{pref} = (706 \pm 11) + (46.6 \pm 0.3)S + (0.00748 \pm 0.00578)\mathrm{PO} - (1.33 \pm 0.06)pT, \qquad \text{(A2)}$$

where $\pm$ indicates a 95% confidence interval for each coefficient. The root mean square error for Alk_{pref} at the surface is 23 μmol kg^{-1}, which may propagate to the estimated error of 12 μmol kg^{-1} for C_{carb}. The globally-averaged value $\overline{C_{carb}}$ is estimated to be 29 ± 12 μmol kg^{-1} where the $\pm$ range reflects the estimate error ($p = 0.05$).

[43] **Acknowledgments.** We thank Daniel Sigman, Mathis Hain and Jess Adkins for constructive and insightful discussions of this work. We also thank François Primeau and Jaime Palter for their review of an earlier version of this manuscript. T.D. would like to thank support from National Science Foundation grant OCE0623647 award to F. Primeau at UCI. E.Y.K.

and J.L.S. acknowledge award NA07OAR4310096 from the National Oceanic and Atmospheric Administration and award ANT-1040957 from the National Science Foundation. The statements, findings, conclusions, and recommendations are those of the authors and do not necessarily reflect the views of the National Oceanic and Atmospheric Administration, or the U.S. Department of Commerce.

References

Ahn, J., and E. J. Brook (2008), Atmospheric CO_2 and climate on millennial time scales during the last glacial period, *Science*, *322*(5898), 83–85.

Anderson, L. A., and J. L. Sarmiento (1994), Redfield ratios of remineralization determined by nutrient data analysis, *Global Biogeochem. Cycles*, *8*(1), 65–80.

Anderson, R. F., et al. (2009), Wind-driven upwelling in the Southern Ocean and the deglacial rise in atmospheric CO_2, *Science*, *323*, 1443–1448.

Archer, D., and E. Maier-Reimer (1994), Effect of deep-sea sedimentary calcite preservation on atmospheric CO_2 concentration, *Nature*, *367*, 260–263.

Archer, D., A. Winguth, D. Lea, and N. Mahowald (2000), What caused the glacial/interglacial atmospheric pCO_2 cycles?, *Rev. Geophys.*, *38*(2), 159–189.

Bouttes, N., D. Paillard, and D. M. Roche (2010), Impact of brine-indueced stratification on the glacial carbon cycle, *Clim. Past*, *6*, 575–589, doi:10.5194/cp-6-575-2010.

Bouttes, N., D. Paillard, D. M. Roche, V. Brovkin, and L. Bopp (2011), Last Glacial Maximum CO_2 and δ13C successfully reconciled, *Geophys. Res. Lett.*, *38*, L02705, doi:10.1029/2010GL044499.

Boyle, E. A. (1988), The role of vertical chemical fractionation in controlling Late Quaternary atmospheric carbon dioxide, *J. Geophys. Res.*, *93*(C12), 15,701–15,714.

Brewer, P. G., G. T. F. Wong, M. P. Bacon, and D. W. Spencer (1975), An oceanic calcium problem? *Earth Planet. Sci. Lett.*, *26*, 81–87.

Broecker, W. S., and T.-H. Peng (1987), The role of $CaCO_3$ compensation in the glacial to interglacial atmospheric CO_2 change, *Global Biogeochem. Cycles*, *1*(1), 15–29.

Cermeño, P., S. Dutkiewicz, R. P. Harris, M. J. Follows, O. Schofield, and P. G. Falkowski (2008), The role of nutricline depth in regulating the ocean carbon cycle, *Proc. Natl. Acad. Sci.*, *105*, 20,344–20,349.

Chikamoto, M. O., K. Matsumoto, and A. Ridgwell (2008), Response of deep-sea $CaCO_3$ sedimentation to Atlantic meridional overturning circulation shutdown, *J. Geophys. Res.*, *113*, G03017, doi:10.1029/2007JG000669.

Chung, S.-N., K. Lee, R. A. Feely, C. L. Sabine, F. J. Millero, R. Wanninkhof, J. L. Bullister, R. M. Key, and T.-H. Peng (2003), Calcium carbonate budget in the Atlantic Ocean based on water column inorganic carbon chemistry, *Global Biogeochem. Cycles*, *17*(4), 1093, doi:10.1029/2002GB002001.

DeVries, T., and F. Primeau (2009), Atmospheric pCO_2 sensitivity to the solubility pump: Role of the low-latitude ocean, *Global Biogeochem. Cycles*, *23*, GB4020, doi:10.1029/2009GB003537.

Dunne, J. P., J. L. Sarmiento, and A. Gnanadesikan (2007), A synthesis of global particle export from the surface ocean and cycling through the ocean interior and on the seafloor, *Global Biogeochem. Cycles*, *20*, GB4006, doi:10.1029/2006GB002907.

Feely, R. A., et al. (2002), In situ calcium carbonate dissolution in the Pacific Ocean, *Global Biogeochem. Cycles*, *16*(4), 1144, doi:10.1029/2002GB001866.

François, R., et al. (1997), Contribution of Southern Ocean surface-water stratification to low atmospheric CO_2 concentrations during the last glacial period, *Nature*, *389*, 929–935.

Garcia, H. E., R. A. Locarnini, T. P. Boyer, and J. I. Antonov (2006), *World Ocean Atlas* 2005, vol. 3, *Dissolved Oxygen, Apparent Oxygen Utilization, and Oxygen Saturation*, *NOAA Atlas NESDIS* 63, edited by S. Levitus, 342 pp., U.S. Govt. Print. Off., Washington, D. C.

Gnanadesikan, A. (1999), A simple theory for the structure of the oceanic pycnocline, *Science*, *283*, 2077–2079.

Goodwin, P., M. J. Follows, and R. G. Williams (2008), Analytical relationships between atmospheric carbon dioxide, carbon emissions, and ocean processes, *Global Biogeochem. Cycles*, *22*, GB3030, doi:10.1029/2008GB003184.

Gruber, N., and J. L. Sarmiento (2002), Large-scale biogeochemical-physical interactions in elemental cycles, in *The Sea*, edited by A. R. Robinson, J. J. McCarthy, and B. J. Rothschild, pp. 337–399, John Wiley, Hoboken, N. J.

Hain, M. P., D. M. Sigman, and G. H. Haug (2010), Carbon dioxide effects of Antarctic stratification, North Atlantic Intermediate Water formation, and subantarctic nutrient drawdown during the last ice age: Diagnosis and synthesis in a geochemical box model, *Global Biogeochem. Cycles*, *24*, GB4023, doi:10.1029/2010GB003790.

Ito, T., and M. J. Follows (2005), Preformed phosphate, soft tissue pump and atmospheric CO_2, *J. Mar. Res.*, *63*, 813–839.

Ito, T., M. J. Follows, and E. A. Boyle (2004), Is AOU a good measure of respiration in the oceans?, *Geophys. Res. Lett.*, *31*, L17305, doi:10.1029/2004GL020900.

Kanamori, S., and H. Ikegami (1982), Calcium-alkalinity relationship in the North Pacific, *Oceanogr. Soc. Jpn*, *38*, 57–62.

Key, R. M., A. Kozyr, C. L. Sabine, K. Lee, R. Wanninkhof, J. L. Bullister, R. A. Feely, F. J. Millero, C. Mordy, and T.-H. Peng (2004), A global ocean carbon climatology: Results from Global Data Analysis Project (GLODAP), *Global Biogeochem. Cycles*, *18*, GB4031, doi:10.1029/2004GB002247.

Knox, F., and M. B. McElroy (1984), Changes in atmospheric CO_2: Influence of the marine biota at high latitude, *J. Geophys. Res.*, *89*, 4629–4637.

Kwon, E. Y., and F. Primeau (2006), Optimization and sensitivity study of a biogeochemistry ocean model using an implicit solver and in situ phosphate data, *Global Biogeochem. Cycles*, *20*, GB4009, doi:10.1029/2005GB002631.

Kwon, E. Y., and F. Primeau (2008), Optimization and sensitivity of a global biogeochemistry ocean model using combined in situ DIC, alkalinity, and phosphate data, *J. Geophys. Res.*, *113*, C08011, doi:10.1029/2007JC004520.

Kwon, E. Y., F. Primeau, and J. L. Sarmiento (2009), The impact of remineralization depth on the air-sea carbon balance, *Nat. Geosci.*, *2*, 630–635.

Lund, D. C., J. F. Adkins, and R. Ferrari (2011), Abyssal Atlantic circulation during the Last Glacial Maximum: Constraining the ratio between transport and vertical mixing, *Paleoceanography*, *26*, PA1213, doi:10.1029/2010PA001938.

Marchitto, T. M., S. J. Lehman, J. D. Ortiz, J. Flückiger, and A. van Geen (2007), Marine radiocarbon evidence for the mechanism of deglacial atmospheric CO_2 rise, *Science*, *316*(5830), 1456–1459.

Marinov, I., M. J. Follows, A. Gnandesikan, J. L. Sarmiento, and R. D. Slater (2008), How does ocean biology affect atmospheric pCO_2? Theory and models, *J. Geophys. Res.*, *113*, C07032, doi:10.1029/2007JC004598.

Martin, J. H., G. A. Knauer, D. M. Karl, and W. W. Broenkow (1987), VERTEX: Carbon cycling in the northeast Pacific, *Deep Sea Res.*, *34*, 267–285.

Najjar, R. G., et al.. (2007), Impact of circulation on export production, dissolved organic matter, and dissolved oxygen in the ocean: Results from Phase II of the Ocean Carbon-cycle Model Intercomparison Project (OCMIP-2), *Global Biogeochem. Cycles*, *21*, GB3007, doi:10.1029/2006GB002857.

Paul, A., and C. Schäfer-Neth (2003), Modeling the water masses of the Atlantic Ocean at the Last Glacial Maximum, *Paleoceanography*, *18*(3), 1058, doi:10.1029/2002PA000783.

Primeau, F. (2005), Characterizing transport between the surface mixed layer and the ocean interior with a forward and adjoint global ocean transport model, *J. Phys. Oceanogr.*, *35*, 545–564.

Robinson, R. S., and D. M. Sigman (2008), Nitrogen isotopic evidence for a poleward decrease in surface nitrate within the ice age Antarctic, *Quat. Sci. Rev.*, *27*(9–10), 1076–1090.

Sabine, C. L., R. M. Key, R. A. Feely, and D. Greeley (2002), Inorganic carbon in the Indian Ocean: Distribution and dissolution processes, *Global Biogeochem. Cycles*, *16*(4), 1067, doi:10.1029/2002GB001869.

Sarmiento, J. L., and N. Gruber (2006), *Ocean Biogeochemical Dynamics*, Princeton Univ. Press, Princeton, N. J.

Sarmiento, J. L., and J. R. Toggweiler (1984), A new model for the role of the oceans in determining atmospheric pCO_2, *Nature*, *308*, 621–624.

Sarmiento, J. L., T. M. C. Hughes, R. J. Stouffer, and S. Manabe (1998), Simulated response of the ocean carbon cycle to anthropogenic climate warming, *Nature*, *393*, 245–249.

Sarmiento, J. L., et al. (2002), A new estimate of the $CaCO_3$ to organic carbon export ratio, *Global Biogeochem. Cycles*, *16*(4), 1107, doi:10.1029/2002GB001919.

Schmittner, A., and E. D. Galbraith (2008), Glacial greenhouse-gas fluctuations controlled by ocean circulation changes, *Nature*, *456*, 373–376, doi:10.1038/nature07531.

Siegenthaler, U., and T. Wenk (1984), Rapid atmospheric CO_2 variations and ocean circulation, *Nature*, *308*, 624–626.

Sigman, D. M., and E. A. Boyle (2000), Gacial/interglacial variations in atmospheric carbon dioxide, *Nature*, *407*, 859–869.

Sigman, D. M., M. P. Hain, and G. H. Haug (2010), The polar ocean and glacial cycles in atmospheric CO_2 concentration, *Nature*, *466*, 47–55.

Skinner, L. C., S. Fallon, C. Waelbroeck, E. Michel, and S. Barker (2010), Ventilation of the deep Southern Ocean and deglacial CO_2 rise, *Science*, *328*(5982), 1147–1151.

Takahashi, T., W. S. Broecker, S. R. Werner, and A. E. Bainbridge (1980), Carbonate chemistry of the surface waters of the world oceans, in *Isotope Marine Chemistry*, edited by E. D. Goldberg, Y. Horibe, and K. Saruhashi, pp. 291–326, Uchida Rokakuho Publ., Tokyo.

Toggweiler, J. R. (1999), Variation of atmospheric CO_2 by ventilation of the ocean's deepest water, *Paleoceanography*, *14*(5), 571–588.

Toggweiler, J. R., and B. L. Samuels (1995), Effect of Drake Passage on the global thermohaline circulation, *Deep Sea Res. I*, *42*(4), 477–500.

Toggweiler, J. R., R. Murnane, S. Carson, A. Gnanadesikan, and J. L. Sarmiento (2003), Representation of the carbon cycle in box models and GCMs: 2, Organic pump, *Global Biogeochem. Cycles*, *17*(1), 1027, doi:10.1029/2001GB001841.

Toggweiler, J. R., J. L. Russell, and S. Carson (2006), Midlatitude westerlies, atmospheric CO_2, and climate change during the ice ages, *Paleoceanography*, *21*, PA2005, doi:10.1029/2005PA001154.

Volk, T., and M. I. Hoffert (1985), Ocean carbon pumps: Analysis of relative strengths and efficiencies in ocean-driven atmospheric CO_2 changes, in *The Carbon Cycle and Atmospheric CO_2: Natural Variations Archean to Present*, *Geophys. Monogr. Ser.*, vol. 32, edited by E. T. Sundquist and W. S. Broecker, pp. 99–110, AGU, Washington, D. C.

Wanninkhof, R. (1992), Relationship between wind speed and gas exchange over the ocean, *J. Geophys. Res.*, *97*, 7373–7382.

Yamanaka, Y., and E. Tajika (1996), The role of the vertical fluxes of particulate organic matter and calcite in the ocean carbon cycle: Studies using an ocean biogeochemical general circulation model, *Global Biogeochem. Cycles*, *10*, 361–382.

Zeebe, R. E., and D. Wolf-Gladrow (2009), CO_2 *in Seawater: Equilibrium, Kinetics, Isotope*, Elsevier, New York.

T. DeVries, Department of Atmospheric and Oceanic Sciences, University of California, Los Angeles, CA 90095, USA. (tdevries@atmos.ucla.edu)

E. Y. Kwon and J. L. Sarmiento, Atmospheric and Oceanic Sciences Program, Princeton University, Princeton, NJ 08544, USA. (ekwon@princeton.edu; jls@princeton.edu)

J. R. Toggweiler, Geophysical Fluid Dynamics Laboratory, NOAA, PO Box 308, Princeton, NJ 08542, USA. (robbie.toggweiler@noaa.gov)